5-26-2007

Hygroscopic Behavior of NaCl-Bearing Natural Aerosol Particles Using Environmental Transmission Electron Microscopy

Matthew E. Wise
Arizona State University, mawise@cu-portland.edu

Trudi A. Semeniuk
Arizona State University

Roelof Bruintjes
National Center for Atmospheric Research

Scot T. Martin
Harvard University

Lynn M. Russell
University of California, San Diego

See next page for additional authors

Authors
Matthew E. Wise, Trudi A. Semeniuk, Roelof Bruintjes, Scot T. Martin, Lynn M. Russell, and Peter R. Buseck

Hygroscopic behavior of NaCl-bearing natural aerosol particles using environmental transmission electron microscopy

Matthew E. Wise,[1] Trudi A. Semeniuk,[1] Roelof Bruintjes,[2] Scot T. Martin,[3] Lynn M. Russell,[4] and Peter R. Buseck[1]

Received 21 June 2006; revised 23 October 2006; accepted 29 January 2007; published 26 May 2007.

[1] We used conventional and environmental transmission electron microscopes to determine morphology, composition, and water uptake of individual natural inorganic aerosol particles collected from industrial pollution plumes and from clean and polluted marine environments. Five particle types are described in detail. They range from relatively insoluble mineral grains to internally mixed particles containing NaCl with other soluble or relatively insoluble material. We studied the hygroscopic behavior of these particles from 0 to 100% relative humidity (RH). Relatively insoluble materials do not take up water over the experimental RH range. Single crystals of NaCl from both natural and laboratory sources have a well-defined deliquescence point of approximately 76% RH at 291 K. NaCl-bearing aggregate particles appear to deliquesce between 74 and 76% RH (same RH within error) when NaCl is internally mixed with relatively insoluble phases, but the particles deliquesce at lower RH when aggregated with other soluble phases such as $NaNO_3$. For all NaCl-bearing particles studied, hygroscopic growth is pronounced above 76% RH, and water uptake by the particles is dominated by the soluble phase. Furthermore, the soluble phase initiating deliquescence controls the locus of further hygroscopic growth of the aggregate particle. Our results demonstrate that composition and mixing state affect water uptake of natural aerosol particles. Furthermore, internally mixed particles are confirmed to deliquesce at lower RH values than predicted from the individual components.

Citation: Wise, M. E., T. A. Semeniuk, R. Bruintjes, S. T. Martin, L. M. Russell, and P. R. Buseck (2007), Hygroscopic behavior of NaCl-bearing natural aerosol particles using environmental transmission electron microscopy, *J. Geophys. Res.*, *112*, D10224, doi:10.1029/2006JD007678.

1. Introduction

[2] Aerosol particles are important components of the atmosphere and influence Earth's climate in a variety of ways through their effects on the radiative budget, atmospheric chemistry, and precipitation. Specifically, the size, composition, and phase (solid or liquid) of an individual aerosol particle affects its ability to scatter and absorb light [e.g., *Charlson et al.*, 1992], to catalyze heterogeneous reactions in the atmosphere [e.g., *Hu and Abbatt*, 1997], and to form cloud condensation nuclei or cloud droplets [e.g., *DeMott and Rogers*, 1990]. All these aspects contribute to uncertainty in global climate models. Ideally, we would like to know the water contents and sizes of different types of aerosol particles over a wide range of atmospheric relative humidity (RH) values.

[3] Electrodynamic balances, infrared absorption cells, optical microscopy, particle mobility analyzers, and environmental scanning electron microscopy have been used to investigate changes in water content and sizes of aerosol particles in both field and laboratory settings. Using these instruments, the hygroscopic behavior of many atmospherically relevant salts such as NaCl and $(NH_4)_2SO_4$ have been studied [e.g., *Biskos et al.*, 2006; *Martin*, 2000; *Tang and Munkelwitz*, 1984; *Tang and Munkelwitz*, 1994]. These studies show a pure salt taking up water to form a solution droplet (deliquescence) at a characteristic RH value (DRH). As the RH increases past the DRH, the particle grows hygroscopically to maintain equilibrium with the water vapor. If the RH decreases, the particle loses water and eventually reforms crystals (efflorescence) at an RH value (ERH) significantly lower than the DRH. Although the experimental techniques used in these studies are sensitive to the water content of the particles, they are not able to determine the morphological changes that submicrometer particles undergo during deliquescence, efflorescence, and hygroscopic growth at varying atmospheric RH values.

[1] School of Earth and Space Exploration and Department of Chemistry and Biochemistry, Arizona State University, Tempe, Arizona, USA.
[2] National Center for Atmospheric Research, Boulder, Colorado, USA.
[3] Division of Engineering and Applied Sciences, Harvard University, Cambridge, Massachusetts, USA.
[4] Scripps Institute of Oceanography, University of California, San Diego, California, USA.

0148-0227/07/2006JD007678

Table 1. Sampling Conditions for Samples Studied With the ETEM

Sample	UAE	ACE-1	SIO
Altitude, m	500	30	10
Temperature, °C	40	9	18
Relative Humidity, %	20	69	21

[4] There are a number of direct measurements of the hygroscopic properties of ambient aerosol particles from the marine boundary layer [*Berg et al.*, 1998; *Carrico et al.*, 2003] and several rural and urban land sites [*Chen et al.*, 2003; *Day and Malm*, 2001; *Malm et al.*, 2003; *Santarpia et al.*, 2005; *Santarpia et al.*, 2004]. Nephelometers and mobility spectrometers were used in these studies to monitor the interaction of ambient aerosol particles with water vapor at various RH values, but these techniques could not simultaneously determine particle composition. Thus, chemical composition has been inferred either from the hygroscopic growth data or from particles sampled (using filters or inertial impactors) and subsequently analyzed by techniques such as ion chromatography.

[5] Environmental scanning electron microscopes (ESEMs) were used in several studies of morphology changes and reactions of individual aerosol particles as a function of RH. *Ebert et al.* [2002] studied the hygroscopic behavior of laboratory-generated NaCl, $(NH_4)_2SO_4$, Na_2SO_4, NH_4NO_3, and ambient soot agglomerates between 0 and 100% RH. *Hoffman et al.* [2004] probed the phase and behavior of laboratory-generated $NaNO_3$ and $NaNO_3$/NaCl particles at various RH values. *Krueger et al.* [2003] exposed particles formed by nebulization of seawater to mixtures of nitric acid and water in the laboratory and then monitored their morphology changes. Finally, *Laskin et al.* [2005] found that hygroscopic calcium nitrate formed when calcite and sea-salt particles reacted with atmospheric nitric acid. Only the last study is of ambient aerosol particles, and that was limited to RH values up to 15% in the ESEM.

[6] The transmission electron microscope (TEM) is a powerful analytical instrument for the study of individual atmospheric aerosol particles because it can resolve chemical and morphological features to the nanometer scale. It can provide information on size, structure, morphology, and composition for each particle. Conventional TEM methods were successfully used to characterize aerosol particles from a variety of sources such as biomass burning, and of source areas such as the marine boundary layer (see reviews by *Buseck et al.* [2002] and *Buseck and Posfai* [1999]). In these studies, analytical techniques including energy-dispersive X-ray spectrometry (EDS) and selected-area electron diffraction (SAED) were used to provide compositions of individual particles and crystallographic information. However, the high vacuum required for conventional TEM operation precludes it from being used to study the effects of changing RH on atmospheric aerosol particles.

[7] An environmental transmission electron microscope (ETEM) can be optimized to study hygroscopic behavior such as phase transitions and morphological changes of individual aerosol particles over the range of RH conditions encountered in the atmosphere. *Wise et al.* [2005] used such an ETEM to observe and accurately measure particle deliquescence and efflorescence of laboratory-generated inorganic salt particles.

[8] A natural progression of this work was to utilize the newly developed capabilities of the ETEM in tandem with conventional TEM analytical techniques (i.e., imaging and EDS). In this way, we were able to determine the composition of a single deposited aerosol particle and to assess its hygroscopic properties. We chose to study an important and ubiquitous class of aerosol particles, namely those that contain NaCl grains, collected from oil-related industrial pollution plumes, clean marine environments, and polluted marine environments. We investigated the behavior of natural NaCl-bearing particles over a range of atmospheric RH values using the ETEM. These samples allowed us to document changes in size and phase of individual aerosol particles from 0 to 100% RH. To our knowledge, this work reports the first compositional, morphological, and hygroscopic measurements of individual natural aerosol particles using a TEM.

2. Experiment

2.1. Laboratory-Generated NaCl Particles

[9] *Wise et al.* [2005] describe the full procedure for salt-particle generation and impaction on TEM substrates. We briefly describe the procedure here. Laboratory-generated NaCl particles used in this study were formed from a 1 M NaCl solution using a TSI model # 3076 atomizer. The particles were next passed through a diffusion dryer (TSI model #3062), which reduced the ambient RH to between ~45 and 65%. The particles were then deposited by diffusion onto a carbon Type-A, 300-mesh Cu (Ted Pella, Inc. #1820) TEM grid.

2.2. Selected Natural Aerosol Particles

[10] We investigated natural aerosol particles from a range of atmospheric environments: oil-related industrial pollution plumes in the United Arab Emirates (UAE, 2002), clean marine aerosol from the Cape Grim Baseline Air Pollution Station in Tasmania (ACE-1, 1995), and polluted marine aerosol from Scripps Pier in San Diego, CA (SIO, 2006). The atmospheric conditions at which the aerosol particles were collected are listed in Table 1.

[11] Aerosol particles were collected directly onto TEM grids using an MPS-3 microanalysis particle sampler (California Instruments, Inc.) for the UAE and SIO sets and a Casella cascade impactor for the ACE-1 field mission. During the UAE field campaign, air was sampled from a low-turbulence inlet on a twin-engine aircraft. For the ACE-1 and SIO sets, the particle sampler drew ambient air from ground-based platforms (tower for ACE-1, pier for SIO). Sampling times varied according to ambient particle concentrations and ranged from 5 to 10 min. Standard Cu-mesh grids with carbon-film substrates (Ted Pella, Inc. #1820, formvar removed) were used. Further information about aerosol sampling in the UAE field campaigns can be found in the work of (T. A. Semeniuk et al., manuscript in preparation, 2007). Details about aerosol sampling in the ACE-1 field campaign can be found in the study of *Posfai et al.* [1999] and *Sievering et al.* [1999].

[12] Using the MPS-3 sampler, we collected size-fractionated aerosol particles on three stages having minimum particle size cut-offs at 2 μm (coarse), 0.3 μm (intermediate), and 0.05 μm (fine). A total of six TEM grids were studied.

2.3. Chemical Analysis of Selected Particles

[13] Initial selection and analysis of individual aerosol particles for each TEM grid was carried out using a Philips CM200 TEM operated at 200 kV. Basic characterization involved bright-field imaging and selected chemical analysis using EDS of over 600 particles to establish dominant particle types and to determine which particle types would provide the most useful information if studied using the ETEM (complete characterization of the particle populations in each source area would have required analyses of many more particles).

[14] We selected a total of 128 particles (from both coarse and fine modes) for ETEM study. The particles on each grid were selected from two regions containing moderate particle loadings. The location of these regions was documented with digital images to allow relocation of the same regions using the ETEM. Typically, 10 particles were selected from each of these regions for ETEM study. Particles were selected spatially close to each other for the practical purpose of rapid translation between particle positions during ETEM experiments, but greater than 0.5 μm apart such that deliquescence spheres of individual particles would not physically contact each other during experiments. Detailed analysis of the $\sim$20 particles per grid for our ETEM experiments first involved imaging under bright-field mode with spot size 1 (25 nm) to document different phases within each particle. After imaging the particles, we performed a qualitative chemical analysis of each phase using EDS with spot size 5 (6.0 nm) to limit beam exposure and beam damage of individual particles. The Philips CM200 TEM provided information on size, shape, composition, speciation, and mixing state for each particle prior to our ETEM experiments, since some of these attributes could be modified during exposure to water vapor. Twenty particles per grid proved to be a feasible number to investigate during a single ETEM experiment.

2.4. Hygroscopic Behavior of Selected Particles

[15] Water uptake experiments were carried out using a 200-kV FEI Tecnai F20 TEM outfitted with a differentially pumped environmental cell. *Wise et al.* [2005] described the ETEM and the experimental procedure developed to study the hygroscopic properties of aerosol particles. We briefly describe modifications to the *Wise et al.* [2005] protocol below.

[16] To determine the RH in the ETEM, we measured the DRH and ERH on standards that consisted of 0.1- to 4-μm NaBr, CsCl, NaCl, $(NH_4)_2SO_4$, and KBr particles at $\sim$18°C. We calibrated RH using the measured DRH and ERH values (from the ETEM) and accepted values (from the literature) for each salt. We ensured that this calibration remained accurate by measuring the DRH of laboratory-generated NaCl particles prior to studying ambient aerosol particles. The DRH measured using the ETEM for the NaCl particles was accurate to at least 2% (theoretical DRH for NaCl = 75.3% [*Richardson and Snyder*, 1994]) for the duration of each experiment.

[17] Water uptake experiments using ambient aerosol particles were initiated by inserting TEM grids into the evacuated ETEM column using a single-tilt sample holder. Sample temperature was regulated through liquid nitrogen cooling and resistive heating and was maintained at $\sim$18°C. This temperature was selected such that a RH of 100% was attained when $\sim$15.5 torr of water vapor was present in the ETEM. Once the temperature was equilibrated ($\sim$5 min), the electron beam was turned on, and the selected particles were relocated (using photographs from the Philips CM200 TEM) and reimaged using the ETEM under vacuum conditions (pressure $<2.2 \times 10^{-5}$ torr). After images and positions of the selected particles were recorded, the electron beam was turned off to limit radiation exposure to the particles. This procedure minimized beam damage and particle heating (see *Wise et al.* [2005] for further discussion).

[18] After initial images and particle positions were recorded at 0% RH, the hygroscopic behavior of each particle over the range 15 to 100% RH was studied. First, we introduced water vapor from a glass bulb containing distilled water at room temperature (via a manual leak valve) into the column. To maintain a constant temperature and a constant RH of 15% in the ETEM, we finely adjusted both water vapor pressure (using the leak valve) and temperature (using the heater in the sample holder). The sample was allowed to equilibrate at these conditions for $\sim$1 min before the electron beam was turned on and each particle was imaged. The process of recording images of each particle at a given RH took $\sim$5 min. Generally, slight movement of the stage occurred after this first step in the ETEM. Therefore particle positions were readjusted before shutting off the electron beam. The RH in the ETEM was then increased to $\sim$40% and the process outlined above was repeated. Images were typically recorded at $\sim$15, 40, 50, 55, 60, 65, 70, 76, 82, 90, and 100% RH for each particle. Water loss by selected particles (for ETEM calibration) was studied using a similar experimental protocol. In this case, the RH was decreased from 100% in a stepwise manner, and images of each particle were typically recorded at $\sim$60, 50, 45, 35, and 0% RH.

3. Results and Discussion

3.1. General Sample Description

[19] Although the particle populations from each of the three sampling sites reflect different local particle sources, each contains a fraction of NaCl-bearing particles. The coarse-mode of the oil-refinery plume sample from the desert region of the UAE is dominated by 2- to 20-μm aggregates of NaCl and mineral dust (T. A. Semeniuk et al., manuscript in preparation, 2007). Typically, NaCl crystals are attached to alumino-silicates, clays, carbonate, or gypsum grains. Single NaCl crystals also are present, and many of the particles are coated with mixed-cation sulfates. These coatings are visible in bright-field mode as well as in EDS spectra. The fine mode of this sample is dominated by mixed-cation sulfate particles, although particle types described in the coarse mode are also present.

[20] Both the coarse- and fine-mode samples of clean marine air from Cape Grim are dominated by approximately 2-μm NaCl particles having attached needles of $CaSO_4$. It is

Table 2. Number of Water-Uptake Experiments Performed on Each Particle Type

Sample	UAE	SIO	ACE-1
Insoluble (i.e, $CaSO_4$)	12	3	1
NaCl	4	2	2
NaCl With Soluble Species	3	6	1
NaCl With Insoluble Species	6	0	16
NaCl With Insoluble and Soluble Species	4	6	14
NaCl With $NaNO_3$, Insoluble, and Soluble Species	0	15	0

possible that they formed upon drying when they reached the TEM grid, but they could also have formed upon drying of ocean spray in the atmosphere. According to M. Pósfai (written communication, 1 May 2006), similar crystals have selected-area electron-diffraction (SAED) patterns that do not match anhydrite ($CaSO_4$) or gypsum ($CaSO_4.2H_2O$). Pósfai believes they may be a hydrated sulfate, with hygroscopic behavior that differs from pure $CaSO_4$.

[21] The coarse-mode of the San Diego polluted marine sample consists of NaCl aggregated with $CaSO_4$, $NaNO_3$ crystals, or silicate grains. Particles are typically 2 to 4 μm in diameter. Single NaCl crystals are also present, and most particles in this sample are coated with a mixed-cation sulfate. The fine mode of this sample is dominated by mixed-cation sulfate particles, although particle types described in the coarse mode are also present.

[22] Seventy-nine of the 128 particles studied with the ETEM contained NaCl, and 16 contained insoluble mineral grains in both the coarse- and fine-grid fractions. The NaCl-bearing particles had variable morphologies and compositions that could be classified into five main particle types: pure NaCl, NaCl with soluble material, NaCl with insoluble material, NaCl with both insoluble and soluble material, and NaCl with other Na salts. The number of water-uptake experiments performed on each particle type and the location where the particles were collected are listed in Table 2.

[23] From the particles studied using the ETEM, we present results for individual coarse-mode particles chosen to show a range of particle phenomena. The aerosol particles presented here range from relatively insoluble single $CaSO_4$ crystals to NaCl-bearing aggregates of soluble or relatively insoluble phases (Figure 1). Each image was recorded using the Philips CM200 TEM at a magnification of 2500 to 5000 times. The specific sites where EDS measurements were taken are denoted by the letters in Figure 1, and the X-ray spectra generated from these measurements are provided in Figure 2. With the exception of spectrum C, all have an X-ray peak characteristic of carbon. This peak results from the carbon substrate and precludes conclusive determination of organic compounds on these grids.

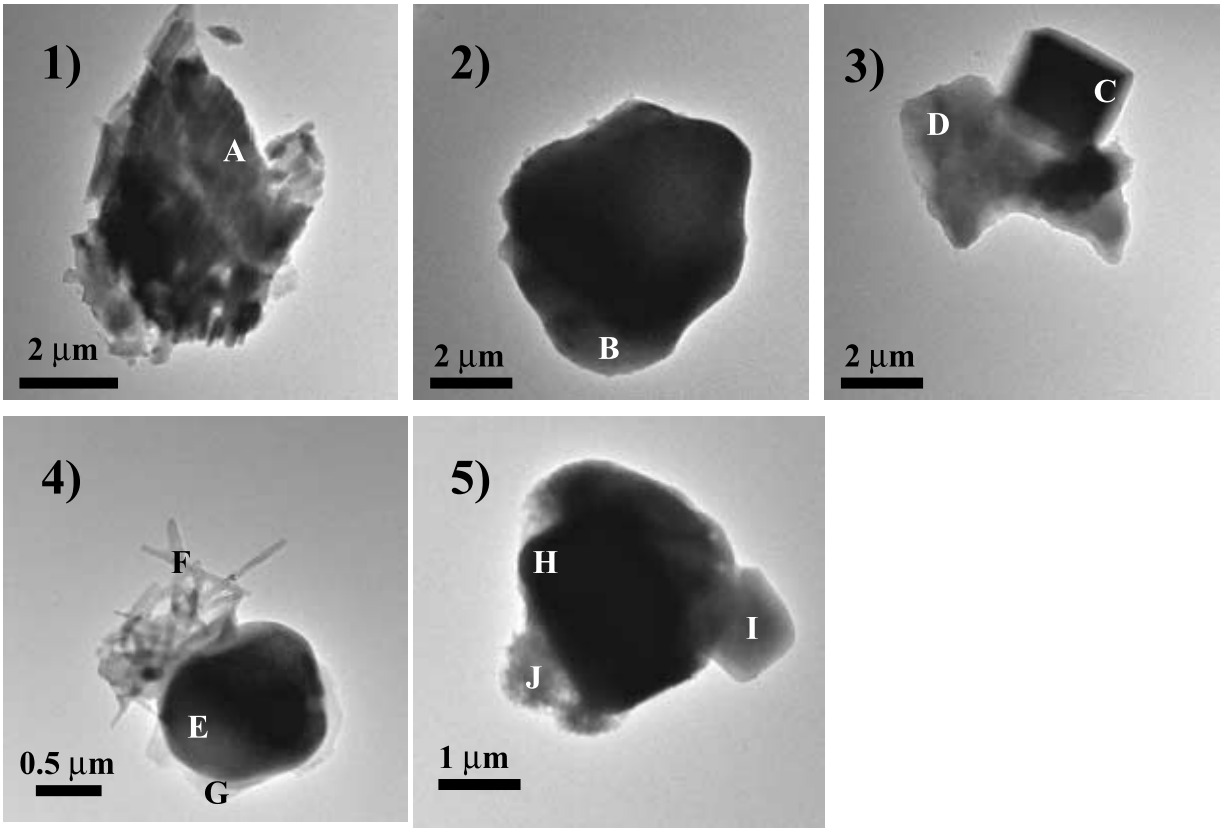

Figure 1. Bright-field images of five particles selected for water uptake studies: (1) $CaSO_4$ grain; (2) NaCl particle; (3) NaCl/mineral dust aggregate; (4) NaCl particle with attached $CaSO_4$ needle crystals; and (5) NaCl particle with attached $NaNO_3$ and $CaSO_4$ crystals. The letters in the figure denote the areas where EDS measurements were obtained to determine particle composition. EDS spectra are shown in Figure 2.

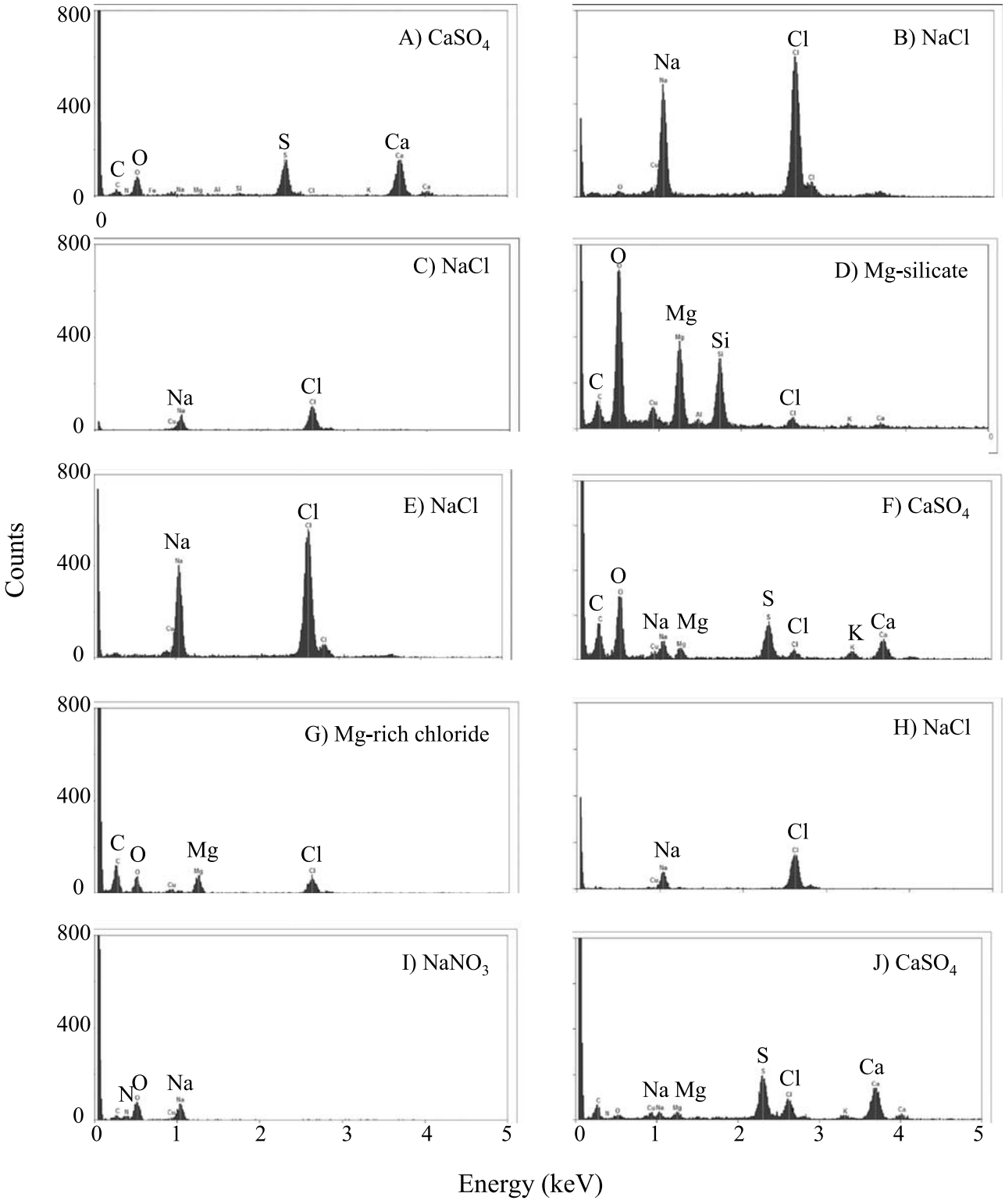

Figure 2. EDS spectra obtained using ES Vision software on the Philips CM200 TEM. Spectra were measured at magnifications around 40,000 times, with beam size 5 (6 nm) for intervals of 10–20 s. EDS measurements at grain boundaries often include a proportion of host grain material. Thus spectra often show mixed compositions (for example, spectra F and J).

[24] Spectrum A in Figure 2, collected from particle 1 (UAE), has peaks characteristic of $CaSO_4$. Spectrum B, recorded from particle 2 (UAE), contains peaks characteristic of NaCl. Particle 3 (UAE) is slightly more complex due to the aggregation of a NaCl grain (spectrum C) and a Mg-silicate grain (spectrum D). Particle 4 (ACE-1) contains a NaCl grain (spectrum E), needle-like $CaSO_4$ crystals (spectrum F), and a coating of Mg- and K-rich chlorides (spectrum G). Spectra

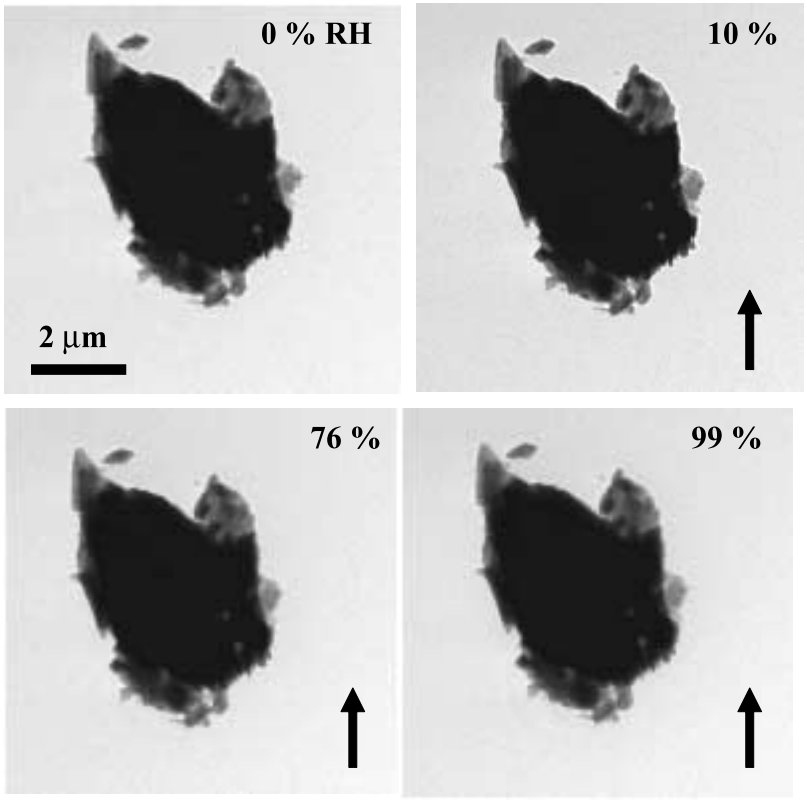

Figure 3. Images of a ~7 μm $CaSO_4$ particle as RH is increased from 10 to 99% RH (denoted by up arrows). The uncertainty in the reported RH values for this and subsequent figures is ±2%.

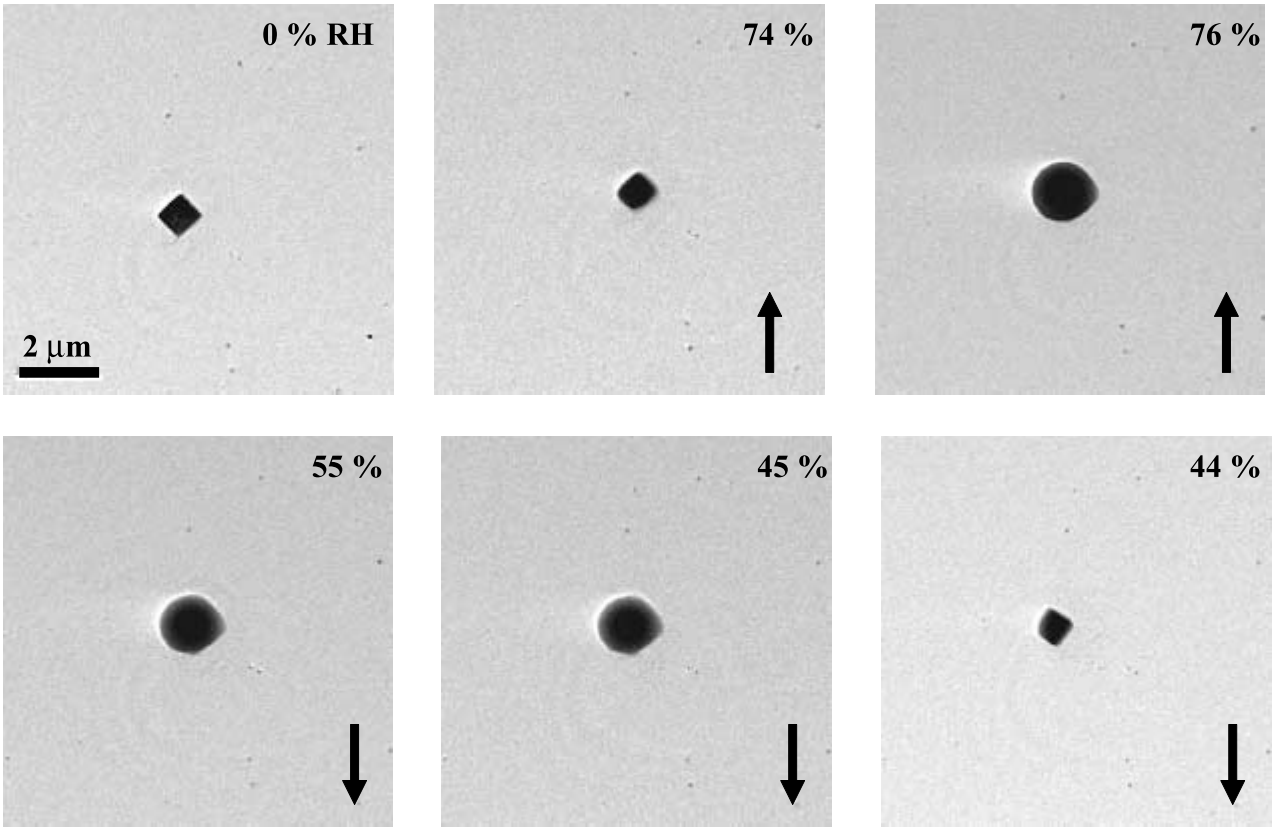

Figure 4. Images of a laboratory-generated NaCl particle (~1 μm) as RH is increased from 0 to 76% and decreased from 76 to 44% (denoted by down arrows).

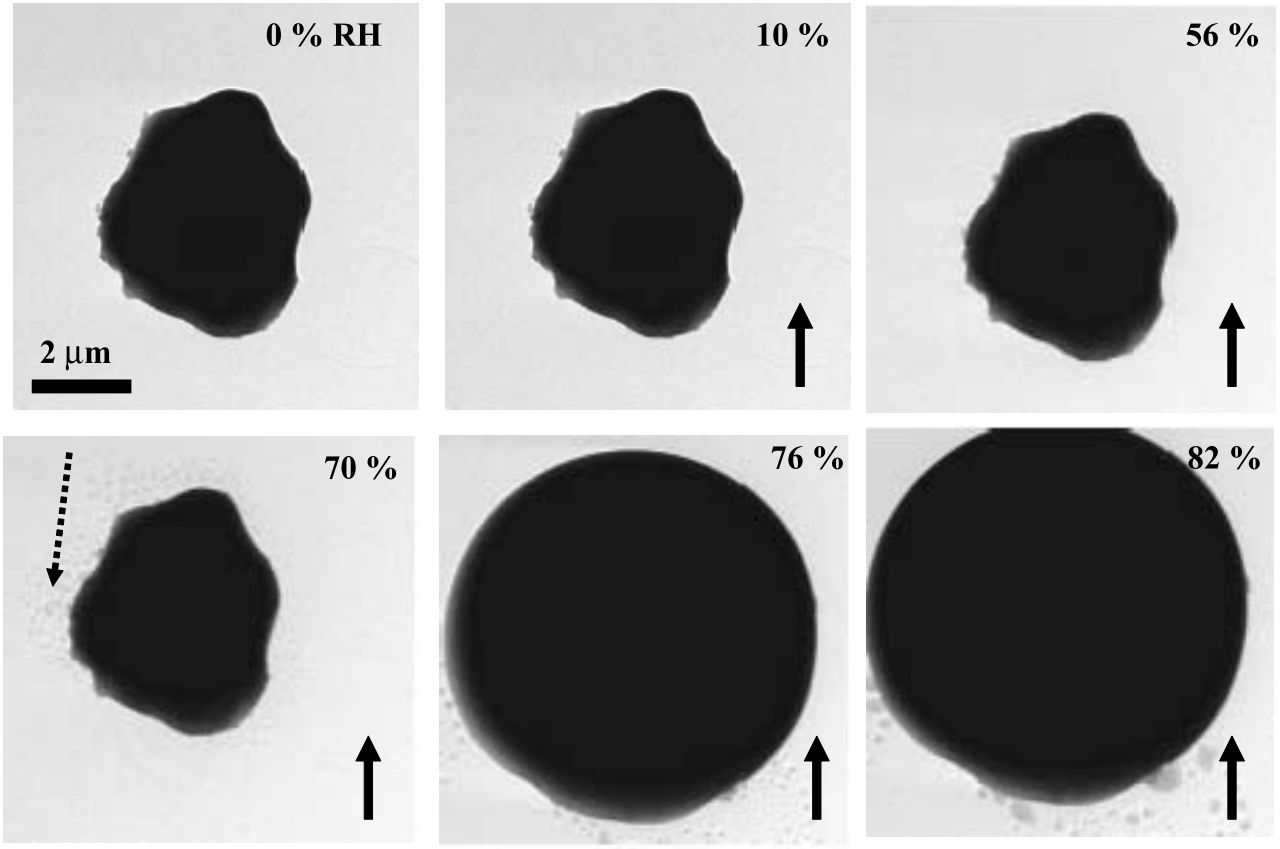

Figure 5. Images of a naturally produced ~5.5-μm NaCl particle as RH is increased from 0 to 82%.

H–J, of particle 5 (SIO) have peaks characteristic of a sea-salt particle collected from polluted marine conditions, i.e., a NaCl core, a $NaNO_3$ crystal, needle-like $CaSO_4$ crystals, and a coating of Mg- and K-rich chlorides and sulfates. This sequence shows increasing chemical complexity from particle 1 to 5.

3.2. Description of the Water Uptake for Particle Types Studied

3.2.1. Natural Particles Containing Relatively Insoluble Substances

[25] Images of a natural gypsum ($CaSO_4 \cdot 2H_2O$) particle, collected during the UAE field campaign, at selected RH values are presented in Figure 3. As the RH is increased in the ETEM from 0 to 99% (indicated by up arrows), the morphology of $CaSO_4$ does not change appreciably. Since gypsum is relatively insoluble (0.205 g/100 g water at 20°C [*Lide*, 2005]), it is not surprising that it does not deliquesce under our experimental conditions. Although the particle does not contain NaCl, it is included in this study to demonstrate the hydrophobic nature of relatively insoluble material at RH values between 0 and 99%.

3.2.2. Laboratory-Generated NaCl Particles

[26] We first determined the behavior of a laboratory-generated NaCl particle at various RH values as a standard for comparison of the behavior of natural particles (Figure 4, see also Figure 2 from *Wise et al.* [2005]). The morphology does not change appreciably as the RH is increased from 0 to 74%. However, at 74% RH the particle boundaries begin to round. At 76% RH it deliquesces and becomes a solution droplet that has a well-defined deliquescence sphere. As the RH is lowered from 76%, the deliquescence sphere shrinks until the ERH of 44% is reached. At this point it recrystallizes. This experiment allows a comparison of the hygroscopic behavior of a pure NaCl particle with natural NaCl-bearing particles. It has deliquescence behavior consistent with suspended NaCl aerosol particles in this size range, and thereby confirms that the ETEM is calibrated (within ±2% RH). The DRH of 76% and the ERH of 44% for the NaCl particle (Figure 4) agree well with the accepted values of ~75 and ~45%, respectively [*Cohen et al.*, 1987a; *Cohen et al.*, 1987b; *Cziczo and Abbatt*, 2000; *Cziczo et al.*, 1997; *Richardson and Snyder*, 1994; *Weis and Ewing*, 1999].

3.2.3. Natural NaCl-Bearing Particles

[27] Relatively pure NaCl particles collected during the UAE field campaign have similar hygroscopic behavior as laboratory-generated NaCl particles, with formation of the main deliquescence sphere at 76% RH and subsequent growth of the sphere at RH > 76% (Figure 5). Although difficult to see in the figure, at 56% RH droplets form on the carbon substrate surrounding the NaCl crystal. The droplets (highlighted by the dashed arrow in the figure) become more apparent as RH is increased to 70%. They form a "splatter zone" surrounding the NaCl particle, which suggests that they originated from the impaction of the particle with the TEM grid. Because the splatter zone begins to take up water prior to the deliquescence point of NaCl, we infer the droplets consisted of something other than NaCl. Although there appears to be a small amount of another soluble phase surrounding (and perhaps on) the NaCl particle, it does not

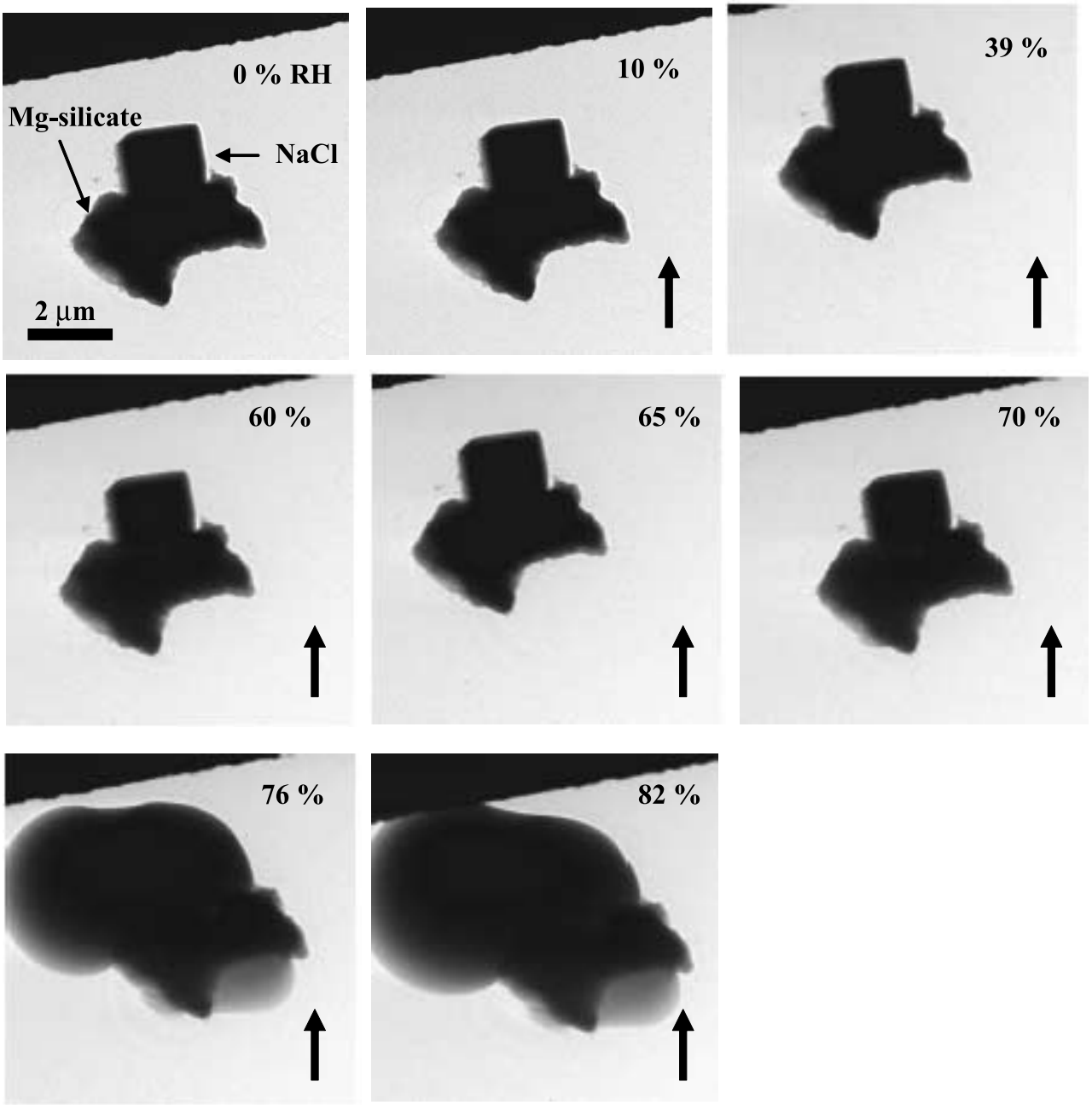

Figure 6. Images of an ~5 μm NaCl particle with an attached Mg-silicate grain as RH is increased from 10 to 82 %.

appear to affect its hygroscopic properties. Furthermore, the phenomenon of droplets appearing on the substrate and surrounding ambient particles at elevated RH values is common (see Figure 3; Semeniuk et al., Water uptake characteristics of individual atmospheric particles having coatings, submitted to Atmospheric Environment, 2007).

[28] Similar hygroscopic properties appear in particles collected from the UAE and Cape Grim (Figures 6 and 7, respectively) that contain NaCl crystals attached to relatively insoluble mineral grains. Images of a NaCl/Mg-silicate particle as RH is increased from 0 to 82% are shown in Figure 6. Although a slight change in morphology occurs at 70% RH, the particle has approximately the same pattern of deliquescence as pure NaCl. The NaCl fully deliquesces at 76% RH, with the deliquescence sphere encompassing the entire aggregate. A NaCl particle with attached $CaSO_4$ needles (Figure 7) changes morphology between 15 and 70% RH. We found that $CaSO_4$ is hydrophobic up to 100% RH and that NaCl morphology does not change appreciably below 70% RH. Therefore we surmise these slight changes in morphology result from the presence of Mg- and K-rich chlorides on the particle surface (see Figure 1, particle 4, area G). Deliquescence of the NaCl crystal occurs as the RH is raised to 74% RH. The deliquescence sphere for each particle in Figures 6 and 7 grows markedly at RH values >75%, engulfing the relatively insoluble material.

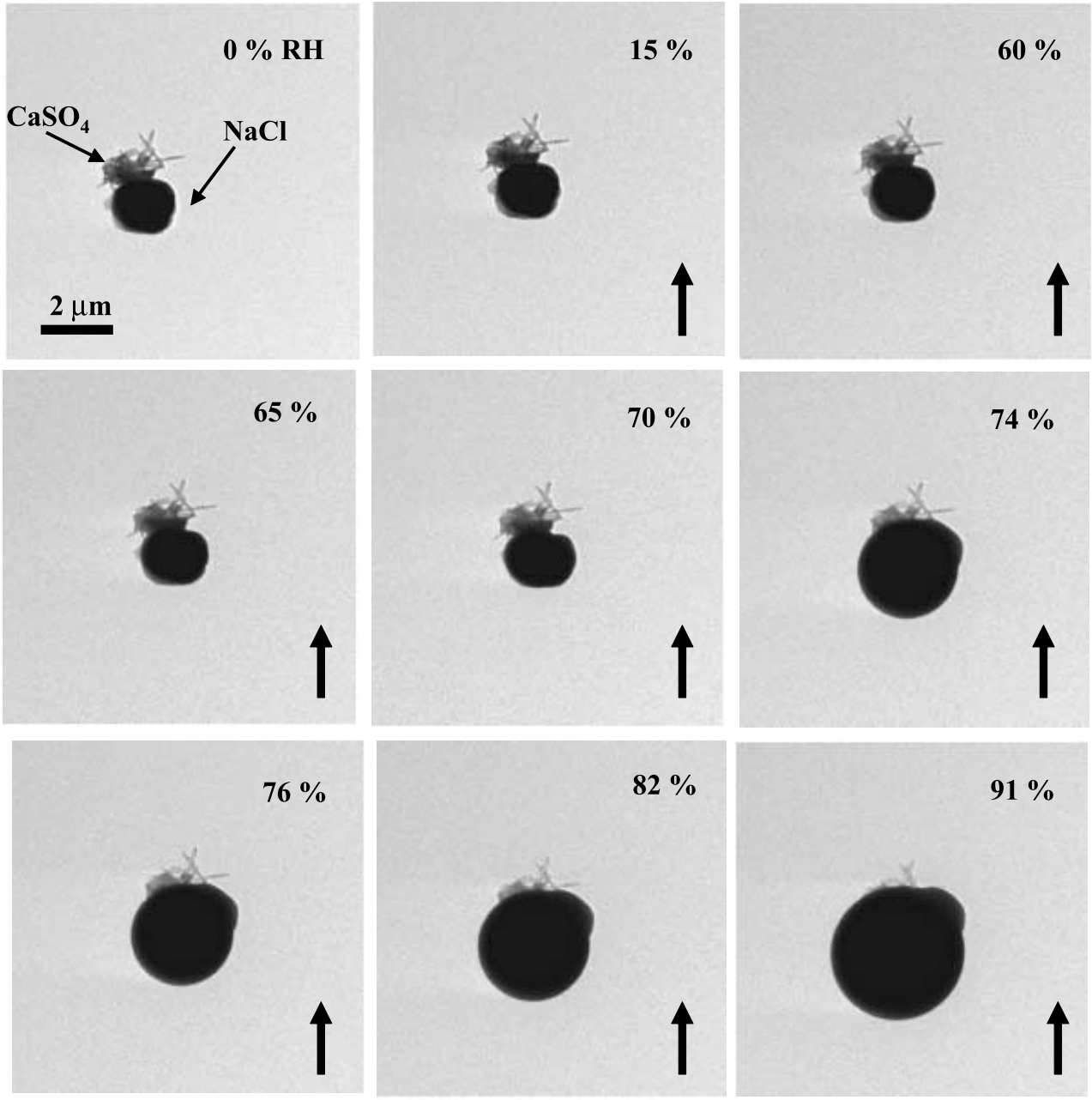

Figure 7. Images of an ~2.7 μm NaCl particle with attached $CaSO_4$ needles as RH is increased from 15 to 91%.

[29] It is well known that the hygroscopic behavior of inorganic particles becomes more complex as additional soluble phases are combined [*Martin*, 2000]. For example, *Tang and Munkelwitz* [1993] show that a particle containing 66% by mass KCl and 33% by mass NaCl has a two-stage deliquescence process, with initial water uptake occurring at 72.7% RH. Pure NaCl and KCl have DRH values of 75.3 and 84.3%, respectively [*Cohen et al.*, 1987a]. Thus, in the *Tang and Munkelwitz* [1993] study, the DRH of a multiphase particle is lower than that of its component phases. Other experimental studies and models dealing with the deliquescence of multiphase aerosol particles corroborate this finding for a multitude of systems [e.g., *Brooks et al.*, 2002; *Clegg et al.*, 2001; *Marcolli et al.*, 2004; *Ming and Russell*, 2002; *Wexler and Seinfeld*, 1991; *Wise et al.*, 2003].

[30] We determined the hygroscopic behavior of a multiphase particle containing NaCl with attached $NaNO_3$ and $CaSO_4$ crystals (SIO, Figure 8). The particle exhibits slightly different hygroscopic behavior from particles previously studied because of the associated $NaNO_3$ (DRH = 74.3% [*Richardson and Snyder*, 1994]). Small changes in morphology occur as the RH increases from 40 to 65% RH, presumably because of the presence of Mg- and K-rich chlorides/sulfates on the particle surface. At 70% RH, a deliquescence sphere forms that we interpret as water uptake by $NaNO_3$. As the RH increases to 75%, NaCl deliquesces and the sphere size increases, in agreement with

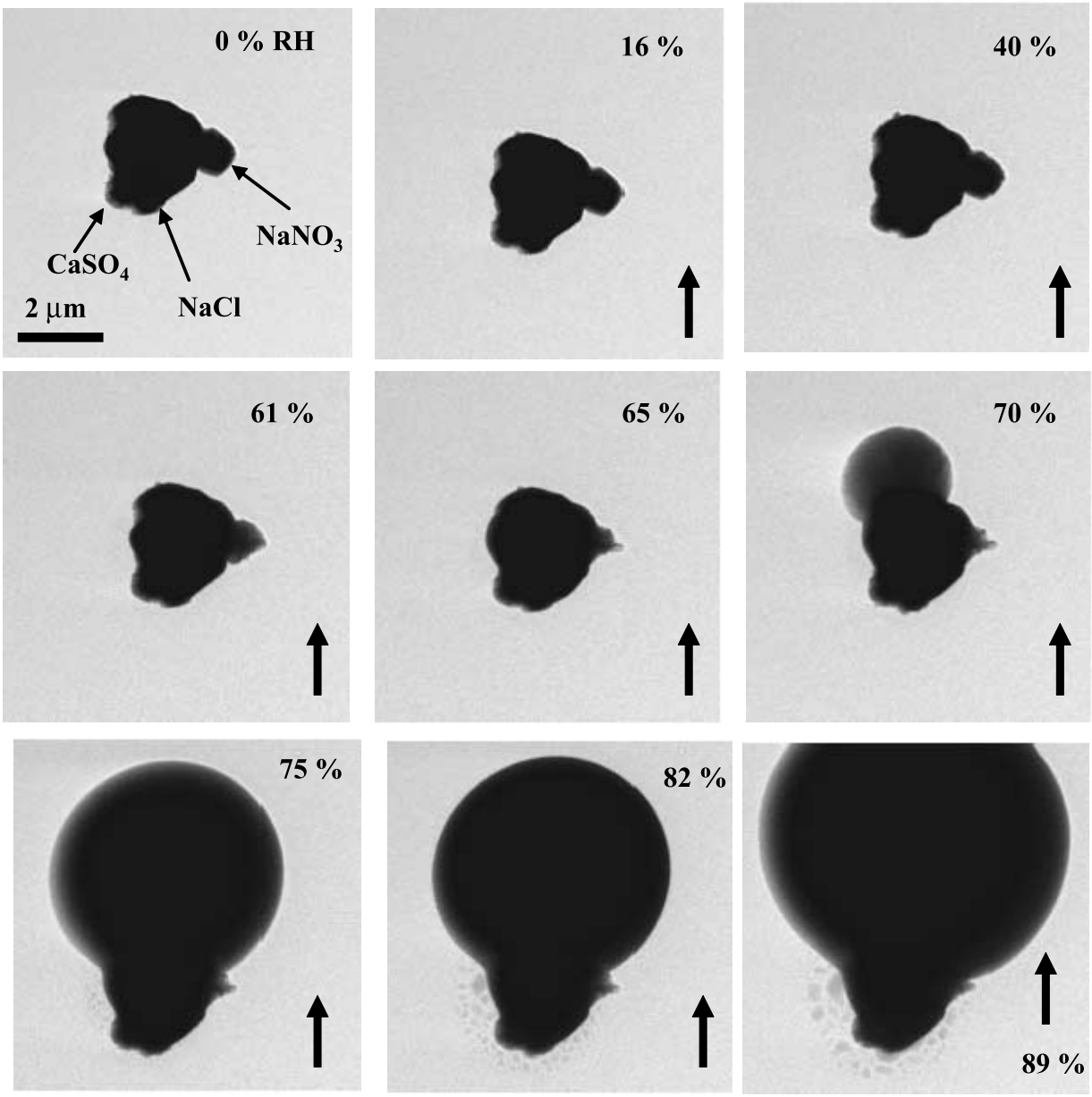

Figure 8. Images of an ~3.6 μm NaCl particle with an attached $NaNO_3$ crystal as RH is increased from 0 to 89%.

the behavior described in laboratory and modeling studies of multiphase inorganic particles. Only one deliquescence sphere develops on the particle, although droplets form around the particle at 75% RH. The $CaSO_4$ crystals did not appear to deliquesce during the experiment.

[31] NaCl dominates hygroscopic growth in the particles in Figures 5, 6, 7, and 8. To calculate growth factors, we must know the contact angle between the particle and the substrate. Future work to determine these contact angles will be needed to provide quantitative estimates of the growth factors of different phases. Even so, the growth factor of NaCl at RH >75% is clearly greater than that of all other phases present. Typically, the deliquescence and subsequent hygroscopic growth of NaCl increases the apparent two-dimensional particle diameter by a factor of ~3 at 100% RH. The shape and location of the deliquescence sphere associated with NaCl varies among particle types. The sphere may engulf the entire particle or it may balloon out from the original particle. Typically, the deliquescence sphere engulfs single NaCl particles and NaCl aggregated with relatively insoluble grains, whereas particles with other soluble phases tend to nucleate growth spheres adjacent to the original particle. This effect probably results from the initiation of deliquescence by the attached soluble phases, with further hygroscopic growth controlled by deliquesced regions of the aggregate particle.

3.2.4. Particles Containing Organic Material

[32] Many natural marine aerosol particles contain relatively insoluble organic compounds such as myristic, stearic, and palmitic acid on their surfaces [*Mochida et al.*, 2003; *Mochida et al.*, 2002; *Russell et al.*, 2002; *Tervahattu et al.*, 2002a; *Tervahattu et al.*, 2002b]. The effects of such relatively insoluble organic coatings on the hygroscopic

properties of marine aerosols are not well understood. Some studies find organic coatings impact the hygroscopic properties of NaCl particles [e.g., *Chen and Lee*, 2001], and others find little to no impact [e.g., *Wagner et al.*, 1996]. The "splatter zone" surrounding the NaCl particle in Figure 5 could indicate the former presence of an organic coating. However, this zone begins to take up water at 56% RH. If the organic coating were relatively insoluble, we would not expect water uptake.

[33] Natural marine aerosol particles can also contain a fraction of soluble organic material within the bulk particle. The effect of such material on the hygroscopic properties of soluble inorganic particles is also not well understood. Although we expect our natural marine aerosol particles to contain organic material, its presence in the NaCl particle in Figure 5 could not be confirmed using EDS. Furthermore, the electron beam in the TEM can damage organic compounds [*Posfai et al.*, 2003]. Thus, other techniques are better suited to determine the effects of soluble organic compounds on the hygroscopic properties of NaCl particles.

4. Summary and Atmospheric Implications

[34] We determined the morphology, composition, and water uptake characteristics of five natural aerosol particles collected from oil-related industrial pollution plumes, clean marine environments, and polluted marine environments between 0 and 100% RH. Particles ranged from single relatively insoluble grains, to single soluble grains, to mixed particles of both soluble and relatively insoluble material. Particles composed of relatively insoluble material, such as $CaSO_4 \cdot 2H_2O$, did not pick up water at RH values up to 100% RH, illustrating the hydrophobic nature of many aerosol particles. Deliquescence of single NaCl crystals, and internal mixtures of NaCl with relatively insoluble material, occurred within the range 74 to 76% RH (same RH within error). This result is consistent with literature values for laboratory-generated NaCl particles. Mixed particles containing NaCl and other soluble material have deliquescence points slightly lower than 74%. This result is also consistent with thermodynamic and laboratory measurements, which find that the DRH of a multicomponent particle is lower than that of its individual components.

[35] Aggregation of soluble and relatively insoluble material in natural aerosol particles changes the way in which they interact with water vapor in the atmosphere. Although relatively insoluble mineral particles, such as $CaSO_4 \cdot 2H_2O$, do not interact with water vapor from 0 to 100% RH, when a relatively insoluble mineral particle is aggregated with a sufficient quantity of soluble material such as NaCl, the NaCl particle will deliquesce and engulf the relatively insoluble mineral, forming a droplet. These observations on aggregates that combine soluble and relatively insoluble phases have implications for both chemical and physical processes in the atmosphere. First, liquid-phase reactions can occur on particles that would otherwise not be active. In general, cloud droplets form when particles reach a critical supersaturation, which depends, in part, on the dry diameter of the particle. If a relatively insoluble particle is attached to NaCl, the initial dry diameter of the particle increases, reducing the supersaturation required for cloud droplet formation and resulting in more rapid droplet formation and larger droplet size.

[36] In addition to enhancing the natural spectra of particles that form droplets, aggregates that contain NaCl undergo dramatic changes in size as a result of hygroscopic growth above 75% RH. The change in size we observe in aggregates that contain both soluble and relatively insoluble phases has implications for their ability to scatter and absorb light. Although our study of water uptake on natural particles supports and corroborates laboratory experiments on simple salts such as NaCl and soluble mixtures containing NaCl, we find that natural particles have even more complex behavior. Mixed particles, coated particles, or both have a great range in chemical and physical behavior. Furthermore, they have a large range in droplet size and hygroscopic growth, reflecting the deliquescence and growth of soluble material in the aggregate particles.

[37] **Acknowledgments.** This material is based upon the work supported by the National Science Foundation under grant 0304213 from the Division of Atmospheric Chemistry. Any opinions, findings, and conclusions or recommendations expressed in this material are those of the authors and do not necessarily reflect the views of the National Science Foundation. We acknowledge use of UAE sample material collected in summer 2002 during phase 1 of the Rainfall Enhancement project funded by the Department of Water Resources Studies, Office of H.H. the President in the UAE and NCAR (sponsored by NSF). The TEM grids used in the UAE field campaign were prepared by Li Jia and Tomoko Kojima, and collected by Vidal Salazar and Tara Jensen. Weather Modification Incorporated of Fargo, North Dakota provided the aircraft. We also acknowledge Herman Sievering for the use of his collected TEM grids during the ACE-1 field campaign. We thank Mihály Pósfai for the help in selecting samples for the study and for a critical review of the manuscript, and Miriam Kastner for access to the Pier at Scripps Institute of Oceanography in San Diego. We gratefully acknowledge the use of the facilities at the John M. Cowley Center for High Resolution Electron Microscopy within the Center for Solid State Science at Arizona State University. In particular, we thank Karl Weiss, John Wheatley, Renu Sharma, and Peter Crozier for their assistance in developing our ETEM technique.

References

Berg, O. H., E. Swietlicki, and R. Krejci (1998), Hygroscopic growth of aerosol particles in the marine boundary layer over the Pacific and Southern Oceans during the First Aerosol Characterization Experiment (ACE 1), *J. Geophys. Res.*, *103*(D13), 16,535–16,545.

Biskos, G., A. Malinowski, L. M. Russell, P. R. Buseck, and S. T. Martin (2006), Nanosize effect on the deliquescence and the efflorescence of sodium chloride particles, *Aerosol Sci. Technol.*, *40*(2), 97–106.

Brooks, S. D., M. E. Wise, M. Cushing, and M. A. Tolbert (2002), Deliquescence behavior of organic/ammonium sulfate aerosol, *Geophys. Res. Lett.*, *29*(19), 1917, doi:10.1029/2002GL014733.

Buseck, P. R., and M. Posfai (1999), Airborne minerals and related aerosol particles: Effects on climate and the environment, *Proc. Natl. Acad. Sci. U. S. A.*, *96*(7), 3372–3379.

Buseck, P. R., D. J. Jacob, M. Posfai, J. Li, and J. R. Anderson (2002), Minerals in the air: An environmental perspective, *Geol. Soc. Am.*, 106–122.

Carrico, C. M., P. Kus, M. J. Rood, P. K. Quinn, and T. S. Bates (2003), Mixtures of pollution, dust, sea salt, and volcanic aerosol during ACE-Asia: Radiative properties as a function of relative humidity, *J. Geophys. Res.*, *108*(D23), 8650, doi:10.1029/2003JD003405.

Charlson, R. J., S. E. Schwartz, J. M. Hales, R. D. Cess, J. A. Coakley, J. E. Hansen, and D. J. Hofmann (1992), Climate forcing by anthropogenic aerosols, *Science*, *255*(5043), 423–430.

Chen, L. Y., F. T. Jeng, C. C. Chen, and T. C. Hsiao (2003), Hygroscopic behavior of atmospheric aerosol in Taipei, *Atmos. Environ.*, *37*(15), 2069–2075.

Chen, Y. Y., and W. M. G. Lee (2001), The effect of surfactants on the deliquescence of sodium chloride, *J. Environ. Sci. Health Part A Toxic/Hazard. Subst. Environ. Eng.*, *36*(2), 229–242.

Clegg, S. L., J. H. Seinfeld, and P. Brimblecombe (2001), Thermodynamic modeling of aqueous aerosols containing electrolytes and dissolved organic compounds, *J. Aerosol Sci.*, *32*(6), 713–738.

Cohen, M. D., R. C. Flagan, and J. H. Seinfeld (1987a), Studies of concentrated electrolyte-solutions using the electrodynamic balance: 1. Water activities for single-electrolyte solutions, *J. Phys. Chem.*, *91*(17), 4563–4574.

Cohen, M. D., R. C. Flagan, and J. H. Seinfeld (1987b), Studies of concentrated electrolyte-solutions using the electrodynamic balance: 3. Solute nucleation, *J. Phys. Chem.*, *91*(17), 4583–4590.

Cziczo, D. J., and J. P. D. Abbatt (2000), Infrared observations of the response of NaCl, $MgCl_2$, NH_4HSO_4, and NH_4NO_3 aerosols to changes in relative humidity from 298 to 238 K, *J. Phys. Chem. A*, *104*(10), 2038–2047.

Cziczo, D. J., J. B. Nowak, J. H. Hu, and J. P. D. Abbatt (1997), Infrared spectroscopy of model tropospheric aerosols as a function of relative humidity: Observation of deliquescence and crystallization, *J. Geophys. Res.*, *102*(D15), 18,843–18,850.

Day, D. E., and W. C. Malm (2001), Aerosol light scattering measurements as a function of relative humidity: A comparison between measurements made at three different sites, *Atmos. Environ.*, *35*(30), 5169–5176.

DeMott, P. J., and D. C. Rogers (1990), Freezing nucleation rates of dilute solution droplets measured between −30°C and −40°C in laboratory simulations of natural clouds, *J. Atmos. Sci.*, *47*, 1056–1064.

Ebert, M., M. Inerle-Hof, and S. Weinbruch (2002), Environmental scanning electron microscopy as a new technique to determine the hygroscopic behaviour of individual aerosol particles, *Atmos. Environ.*, *36*(39–40), 5909–5916.

Hoffman, R. C., A. Laskin, and B. J. Finlayson-Pitts (2004), Sodium nitrate particles: Physical and chemical properties during hydration and dehydration, and implications for aged sea salt aerosols, *J. Aerosol Sci.*, *35*(7), 869–887.

Hu, J. H., and J. P. D. Abbatt (1997), Reaction probabilities for N_2O_5 hydrolysis on sulfuric acid and ammonium sulfate aerosols at room temperature, *J. Phys. Chem. A*, *101*(5), 871–878.

Krueger, B. J., V. H. Grassian, M. J. Iedema, J. P. Cowin, and A. Laskin (2003), Probing heterogeneous chemistry of individual atmospheric particles using scanning electron microscopy and energy-dispersive X-ray analysis, *Anal. Chem.*, *75*(19), 5170–5179.

Laskin, A., M. J. Iedema, A. Ichkovich, E. R. Graber, I. Taraniuk, and Y. Rudich (2005), Direct observation of completely processed calcium carbonate dust particles, *Faraday Discuss.*, *130*, 453–468.

Lide, D. R. (2005), CRC Handbook of chemistry and physics, pp. 2544, The Chemical Rubber Company, Cleveland.

Malm, W. C., D. E. Day, S. M. Kreidenweis, J. L. Collett, and T. Lee (2003), Humidity-dependent optical properties of fine particles during the Big Bend regional aerosol and visibility observational study, *J. Geophys. Res.*, *108*(D9), 4279, doi:10.1029/2002JD002998.

Marcolli, C., B. P. Luo, and T. Peter (2004), Mixing of the organic aerosol fractions: Liquids as the thermodynamically stable phases, *J. Phys. Chem. A*, *108*(12), 2216–2224.

Martin, S. T. (2000), Phase transitions of aqueous atmospheric particles, *Chem. Rev.*, *100*(9), 3403–3454.

Ming, Y., and L. Russell (2002), Thermodynamic equilibrium of organic-electrolyte mixtures in aerosol particles, *AIChE J.*, *48*(6), 1331–1348.

Mochida, M., Y. Kitamori, K. Kawamura, Y. Nojiri, and K. Suzuki (2002), Fatty acids in the marine atmosphere: Factors governing their concentrations and evaluation of organic films on sea-salt particles, *J. Geophys. Res.*, *107*(D17), 4325, doi:10.1029/2001JD001278.

Mochida, M., K. Kawamura, N. Umemoto, M. Kobayashi, S. Matsunaga, H. J. Lim, B. J. Turpin, T. S. Bates, and B. R. T. Simoneit (2003), Spatial distributions of oxygenated organic compounds (dicarboxylic acids, fatty acids, and levoglucosan) in marine aerosols over the western Pacific and off the coast of East Asia: Continental outflow of organic aerosols during the ACE-Asia campaign, *J. Geophys. Res.*, *108*(D23), 8638, doi:10.1029/2002JD003249.

Posfai, M., J. R. Anderson, P. R. Buseck, and H. Sievering (1999), Soot and sulfate aerosol particles in the remote marine troposphere, *J. Geophys. Res.*, *104*(D17), 21,685–21,693.

Posfai, M., R. Simonics, J. Li, P. V. Hobbs, and P. R. Buseck (2003), Individual aerosol particles from biomass burning in southern Africa: 1. Compositions and size distributions of carbonaceous particles, *J. Geophys. Res.*, *108*(D13), 8483, doi:10.1029/2002JD002291.

Richardson, C. B., and T. D. Snyder (1994), A study of heterogeneous nucleation in aqueous-solutions, *Langmuir*, *10*(7), 2462–2465.

Russell, L. M., S. F. Maria, and S. C. B. Myneni (2002), Mapping organic coatings on atmospheric particles, *Geophys. Res. Lett.*, *29*(16), 1779, doi:10.1029/2002GL014874.

Santarpia, J. L., R. J. Li, and D. R. Collins (2004), Direct measurement of the hydration state of ambient aerosol populations, *J. Geophys. Res.*, *109*(D18), D18209, doi:10.1029/2004JD004653.

Santarpia, J. L., R. Gasparini, R. J. Li, and D. R. Collins, Diurnal variations in the hygroscopic growth cycles of ambient aerosol populations (2005), *J. Geophys. Res.*, *110*(D3), D03206, doi:10.1029/2004JD005279.

Sievering, H., B. Lerner, J. Slavich, J. Anderson, M. Posfai, and J. Cainey (1999), O-3 oxidation of SO2 in sea-salt aerosol water: Size distribution of non-sea-salt sulfate during the First Aerosol Characterization Experiment (ACE 1), *J. Geophys. Res.*, *104*(D17), 21,707–21,717.

Tang, I. N., and H. R. Munkelwitz (1984), An investigation of solute nucleation in levitated solution droplets, *J. Colloid Interface Sci.*, *98*(2), 430–438.

Tang, I. N., and H. R. Munkelwitz (1993), Composition and temperature-dependence of the deliquescence properties of hygroscopic aerosols, *Atmos. Environ.*, *27*(4), 467–473.

Tang, I. N., and H. R. Munkelwitz (1994), Aerosol phase-transformation and growth in the atmosphere, *J. Appl. Meteorol.*, *33*(7), 791–796.

Tervahattu, H., K. Hartonen, V. M. Kerminen, K. Kupiainen, P. Aarnio, T. Koskentalo, A. F. Tuck, and V. Vaida (2002a), New evidence of an organic layer on marine aerosols, *J. Geophys. Res.*, *107*(D7), 4053, doi:10.1029/2000JD000282.

Tervahattu, H., J. Juhanoja, and K. Kupiainen (2002b), Identification of an organic coating on marine aerosol particles by TOF-SIMS, *J. Geophys. Res.*, *107*(D16), 4319, doi:10.1029/2001JD001403.

Wagner, J., E. Andrews, and S. M. Larson (1996), Sorption of vapor phase octanoic acid onto deliquescent salt particles, *J. Geophys. Res.*, *101*(D14), 19,533–19,540.

Weis, D. D., and G. E. Ewing (1999), Water content and morphology of sodium chloride aerosol particles, *J. Geophys. Res. Atmos.*, *104*(D17), 21,275–21,285.

Wexler, A., and J. H. Seinfeld (1991), Second-generation inorganic aerosol model, *Atmos. Environ.*, *25A*(12), 2731–2748.

Wise, M. E., J. D. Surratt, D. B. Curtis, J. E. Shilling, and M. A. Tolbert (2003), Hygroscopic growth of ammonium sulfate/dicarboxylic acids, *J. Geophys. Res.*, *108*(D20), 4638, doi:10.1029/2003JD003775.

Wise, M. E., G. Biskos, S. T. Martin, L. M. Russell, and P. R. Buseck (2005), Phase transitions of single salt particles studied using a transmission electron microscope with an environmental cell, *Aerosol Sci. Technol.*, *39*, 849–856.

R. Bruintjes, National Center for Atmospheric Research, Boulder, CO 80301, USA.

P. R. Buseck, T. A. Semeniuk, and M. E. Wise, School of Earth and Space Exploration, Arizona State University, Tempe, AZ 85287, USA. (matthew.wise@asu.edu)

S. T. Martin, Division of Engineering and Applied Sciences, Harvard University, Cambridge, MA 02138, USA.

L. M. Russell, Scripps Institute of Oceanography, University of California, San Diego, La Jolla, CA 92093, USA.